Chemical Engineering Journal 351 (2018) 867–877

Contents lists available at ScienceDirect

Chemical Engineering Journal

journal homepage: www.elsevier.com/locate/cej

Destruction of phenicol antibiotics using the UV/H_2O_2 process: Kinetics, byproducts, toxicity evaluation and trichloromethane formation potential

Kai Yin[a,b,1], Lin Deng[b,c,1], Jinming Luo[b,*], John Crittenden[b], Chengbin Liu[a], Yuanfeng Wei[a], Longlu Wang[a]

[a] State Key Laboratory of Chemo/Biosensing and Chemometrics, Hunan University, Changsha 410082, PR China
[b] Brook Byers Institute for Sustainable Systems and School of Civil and Environmental Engineering, Georgia Institute of Technology, 828 West Peachtree Street, Atlanta, GA 30332, United States
[c] Key Laboratory of Building Safety and Energy Efficiency, Ministry of Education, Department of Water Engineering and Science, College of Civil Engineering, Hunan University, Changsha, Hunan 410082, PR China

HIGHLIGHTS

- A pseudo-steady-state model was established to predict PABs degradation.
- A degradation pathway via HO·-triggering was proposed.
- Antimicrobial property, acute toxicity and ecotoxicity were evaluated.
- Extending irradiation time for UV/H_2O_2 process was favor of reducing TCMFP due to low DOC.

GRAPHICAL ABSTRACT

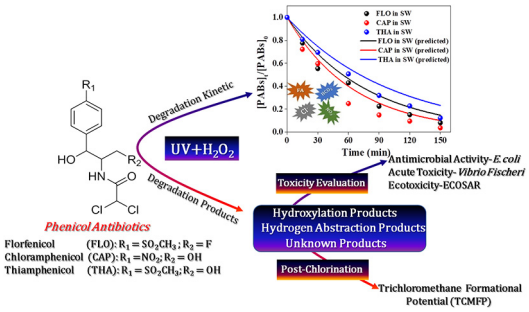

ARTICLE INFO

Keywords:
Phenicol antibiotics
Kinetic modeling
Degradation mechanism
Toxicity evaluation
Trichloromethane

ABSTRACT

Phenicol antibiotics (PABs) degradation by UV/H_2O_2 is important because we need to determine the reduction in toxicity and disinfection byproducts for post-chlorine. In this study, the degradation of PABs, including florfenicol (FLO), chloramphenicol (CAP) and thiamphenicol (THA), was examined. The pseudo-first order degradation rate constants of PABs were 3 times higher in ultrapure water (UW) than that in synthetic wastewater (SW) for these conditions: $[PABs]_0$ = 1 μM, $[H_2O_2]$ = 0.1 mM, and $I_0 = 1.985 \times 10^{-6}$ E L^{-1} s^{-1}. Fulvic acid (FA) and HCO_3^- inhibited PABs degradation, Cl^- and NO_3^- concentrations of up to 5 mM and 10 mM had a negligible impact. The impact of water matrix on PABs degradation was successfully predicted using pseudo-steady-state kinetic model. The degradation of PABs was triggered via hydroxylation and/or hydrogen abstraction. The treatment of PABs via UV/H_2O_2 could decrease their antimicrobial properties, while the byproducts of FLO and THA showed higher acute toxicity in *Vibrio fischeri*. In addition, two identification products (TP-276 and TP-354) of FLO had higher ecotoxicity toxicity (using ECOSAR) in fish, daphnid and green algae. The trichloromethane formation potential (TCMFP) for PABs with post-chlorination in UW and SW can be reduced after UV/H_2O_2 compared to UV, and is related to the corresponding decrease of dissolved organic carbon (DOC).

* Corresponding author.
E-mail address: jinming.luo@ce.gatech.edu (J. Luo).
[1] The authors contributed equally to this work.

https://doi.org/10.1016/j.cej.2018.06.164
Received 25 March 2018; Received in revised form 24 June 2018; Accepted 25 June 2018
Available online 25 June 2018
1385-8947/

1. Introduction

Phenicol antibiotics (PABs), including florfenicol (FLO), chloramphenicol (CAP) and thiamphenicol (THA), are widely used to inhibit disease in both human and livestock aquaculture [1,2]. The overuse of antimicrobial agents has created the risk of transferring antibiotic resistance to pathogenic microbes [3–5]. Meanwhile, PABs have been frequently detected in various aquatic environments and may eventually be present in drinking water sources [6,7]. PABs are very stable [8], and difficult to degrade by conventional water treatment technologies, such as biological processes, filtration, coagulation, flocculation and sedimentation [9–11]. Thus, it is urgent to remove PABs from wastewater before being discharged into aquatic environments.

Advanced oxidation processes (AOPs) are an attractive and promising technology to eliminate organic contaminants. In particular, the combination of ultraviolet light with hydrogen peroxide (UV/H_2O_2) has been frequently utilized to destruct organic pollutants in water by creating highly reactive hydroxyl radical (HO·) [12–15]. Even so, it remains difficult to completely mineralize pollutants over the typical operation time, and a number of byproducts may persist in water [15,16]. The byproducts may have much lower activity [13,17] or retain the properties of the parent compounds (e.g., antimicrobial nature) and potentially become biologically active [18,19]. Furthermore, the toxicity of byproducts may exceed the parent compounds [20]. Therefore, identifying the reaction mechanism and measuring the toxicity of products are an indispensable part of evaluating the UV/H_2O_2 process. However, the current toxicity evaluation of byproducts and parent molecules has focused mainly on a single bioassay (e.g., antimicrobial property, acute toxicity or ecotoxicity). This is inadequate to obtain a comprehensive understanding of the change in toxicity and provide practical guidelines. Additionally, undesirable disinfection by-products (DBPs), including trichloromethane (TCM) can be formed during post-chlorination of PABs after UV/H_2O_2 treatment and this need to be considered [21,22]. Meanwhile, theoretical calculations (e.g., density functional theory) can identify whether target organic pollutants can be efficiently degraded by oxidizing species [23]. To the best of our knowledge, there has no been theoretical calculation on the reactivity of PABs by radical attack or direct photolysis using UV/H_2O_2 process. Water constituents in actual wastewater could affect the efficacy of UV/H_2O_2 process, thus establishing a suitable mathematical model to predict their impact is highly valuable [15,24,25]. Therefore, a comprehensive understanding of the UV/H_2O_2 process is needed that determined the (1) degradation kinetics, (2) byproducts and pathways, (3) change to toxicity and (4) TCM formation potential (TCMFP).

In this study, we examined the impacts of operational variables, such as PABs concentration, H_2O_2 dose, and matrix species (including fulvic acid (FA), HCO_3^-, Cl^- and NO_3^-), on PABs degradation. The relationship between the degradation efficiency and electronic structure of PABs was confirmed by density functional theory (DFT). A pseudo-steady-state kinetic model was established to predict the impact of water constituents on PABs degradation. Meanwhile, the initial fate of PABs via UV/H_2O_2 process was investigated to uncover their destruction pathways. The toxicity of the parent compounds and their byproducts was comprehensively evaluated by antimicrobial property, acute toxicity and ecotoxicity. The TCMFP in post-chlorination was investigated on PABs after UV and UV/H_2O_2 pretreatment.

2. Materials and methods

2.1. Chemicals

FLO, CAP, THA and *p*-chlorobenzoic acid (*p*CBA) were purchased from Aladdin (Shanghai, China). The structures and chemical properties of the antibiotics are shown in Table S1 in the Supporting Information. Ultrapure water (18.2 MΩ·cm) was obtained from a Ulupure water purification system. Hydrogen peroxide solutions were prepared by diluting H_2O_2 (30% w/w) with ultrapure water, which was standardized by the I_3^- method [26]. Other chemical reagents were analytical grade and obtained from Sinopharm Chemical Reagent Co., Ltd (Shanghai, China). The stock solutions (0.1 mM) of FLO, CAP and THA were separately prepared with ultrapure water. Prior to the tests, the stock solution was diluted to a desired concentration.

2.2. Experimental procedure

A collimated beam apparatus (Fig. S1), consisting of one 15 W low-pressure mercury lamp above a quartz reactor, was employed for the batch UV/H_2O_2 studies. Water samples were irradiated and withdrawn at a scheduled interval. A minimum of one hour of warm-up time ensured a stabilized UV emission output. The oxidation was initiated after adding appropriate volumes of H_2O_2 stock solution by stirring (250 r min^{-1}) at room temperature (approximately 25 °C) under UV irradiation. The treatment process with UV alone was conducted as a control under similar conditions.

After the PAB solution was treated by UV/H_2O_2 or UV (initial concentration of PABs = 3 μM, H_2O_2 = 0.3 mM), the PAB reaction solution was further treated with enough chlorination for 24 h in the dark (Cl_2 dose = 1.0 mM). After the chlorination, the disinfectant residual was quenched with ascorbic acid (2.0 mM) [27,28]. The disinfection by-product TCM was analyzed with a static headspace and gas chromatography/mass spectrometry (GC/MS) (Trace2000 Polaris Q). TCM yield was determined according to Eq. (1).

$$\text{TCM yield} = \frac{\text{Formed TCM molar concentration}}{\text{Initial PAB molar concentration}} \times 100\% \quad (1)$$

2.3. Analytical methods

A determination method was used, which included solid-phase extraction (SPE), high-performance liquid chromatography (HPLC), and triple quadrupole mass spectrography (tqMS) (Agilent Technology 1290/6460) with electron spray ionization (ESI) using multiple reaction monitoring (MRM) in the negative mode. The detection limits for FLO, CAP, THA, and TCM were all below 0.1 μg/L. Detailed information about the operation procedures, conditions and parameters is provided in Text S1 and Table S2.

2.4. Calculation of frontier electron densities (FEDs)

All the calculations based on DFT were performed using the DMol3 package with the Perdew-Burke-Ernzerhof/Double-Numerical Dasis 4.4 set. All computations converged upon a true energy minimum, which was confirmed by the absence of imaginary frequencies. The cutoff radius was 4 Å.

2.5. Toxicity tests

The antimicrobial property of the PABs and their byproducts were tested using the *Escherichia coli* bacteria. Because standards of byproducts are not commercially available, it is difficult to assess the toxicity of the products individually. Instead, a sample aliquot was taken from the reaction mixture of PABs in UW via UV/H_2O_2 at each selected time interval. Luria Bertani (LB) broth was used for activation and culturing. After mixing the LB broth with the samples containing parent PABs or byproducts, *Escherichia coli* was incubated in an incubator rotating under 160 rpm at 37 °C for 7 h. OD_{600} (optical density at 600 nm wavelength) was used as an indication of bacterial growth. The acute toxicity assay was carried out against marine luminescent bacterium *Vibrio fischeri*. Quantitative structure-activity relationship (QSAR) analysis, as calculated by the Ecological Structure-Activity Relationship Model (ECOSAR) program, was employed to assess the acute and chronic toxicity for fish, daphnid and green algae.

3. Results and discussion

3.1. Degradation of PABs by UV/H_2O_2

The degradation of PABs by UV/H_2O_2 process includes two parts: (i) direct photolysis (via UV irradiation) and (ii) indirect photolysis (reactive radical species). To determine the contribution of indirect photolysis during UV/H_2O_2 process, the degradation of PABs by UV alone was first studied in the ultrapure water (UW, buffered by phosphate) and synthetic wastewater (SW, constituents are shown in Table S3). The degradation efficiencies of FLO, CAP and THA by UV were 33.67, 51.38 and 25.64% in UW and 31.61, 42.93 and 24.77% in SW after 30 min of reaction time, respectively (Fig. S2A and S2B). The degradation of PABs in both UW and SW follows the pseudo-first-order kinetics. Based on the Lambert-Beers law, the photolysis rate can be written as shown in theoretical kinetic equation is defined as Eq. (2). When the UV absorbance of the reaction solution is very low (i.e., $2.303\varepsilon_{\lambda}bC < 0.02$), Eq. (2) can be simplified as Eq. (3) using a Taylor series expansion using the first term [29]. The quantum yield of the PABs can be calculated according to Eq. (4).

$$-\frac{dC}{dt} = \Phi_{254\ nm} I_o (1-e^{-2.303\varepsilon_{254\ nm} bC}) \quad (2)$$

$$-\frac{dC}{dt} = 2.303\Phi_{254\ nm} I_o \varepsilon_{254\ nm} bC = kC \quad (3)$$

$$\Phi_{254\ nm} = \frac{k}{2.303 I_o \varepsilon_{254\ nm} b} \quad (4)$$

where C is the PABs concentration (M), dC/dt is the degradation rate of PABs (M s^{-1}), Φ_{254nm} is the quantum yield at the wavelength of 254 nm (mol·Einstein^{-1}), I_o is the volumetric light irradiance (E L^{-1} s^{-1}), ε_{254nm} is the molar absorption coefficient at the wavelength of 254 nm (M^{-1} cm^{-1}), b is the optical path length (cm), and k is the first-order rate constant (s^{-1}). The I_o and b in this study (Text S2) were determined as 1.985×10^{-6} E L^{-1} s^{-1} (Fig. S3) and 0.63 cm (Fig. S4), respectively. Other values are listed in Table 1. The ε_{254nm} values of PABs were in the range of 1.235×10^4–1.435×10^4 M^{-1} cm^{-1}. The direct photolysis of PABs is feasible due to their UV absorbance. The first-order rate constants (k_d) of PABs degradation ranged from 1.65×10^{-4} to 3.87×10^{-4} s^{-1} and 1.66×10^{-4} to 3.23×10^{-4} s^{-1} in UW and SW, respectively, and followed the order of CAP > FLO > THA.

During direct photolysis, molecules absorb photons, and electrons are excited to a higher energy state, which enables structural change and leads to the degradation of parent compounds. Therefore, the overall transformation of PABs by direct photolysis under UV 254 nm depends on (i) the ability of PABs to absorb UV light and (ii) the possibility of structural transformation after UV light absorption. Meanwhile, the ability to absorb UV light depends on the electron distribution of molecules. The high molar absorption coefficient of the PABs is mainly attributed to their conjugated aromatic structure. The *p* orbit in the conjugated aromatic structure can enhance light absorption by lowering energy barrier between ground and excited states [30]. The degradation rates of PABs in SW are closed to those in UW, indicating that the components in SW showed a negligible influence in the direct photolysis of PABs might due to the low light absorption of the components at 254 nm (Fig. S5). In addition, the degradation of PABs was negligible when only using H_2O_2 (Fig. S6), indicating that oxidation of PABs by H_2O_2 alone is unable to destroy PABs [31].

Table 1
Molar absorption coefficient (ε), quantum yield (Φ) and direct photolysis rate constants (k_d) for PAB degradation by UV alone.

Species	ε_{254nm} (M^{-1}·cm^{-1})[a]	Φ_{254nm} (mol·Einstein^{-1})[b]	k_d ($\times 10^{-4}$ s^{-1}) (in UW)	k_d ($\times 10^{-4}$ s^{-1}) (in SW)
FLO	1.235×10^4	6.115×10^{-3}	2.18 ± 0.32	1.98 ± 0.48
CAP	1.435×10^4	7.027×10^{-3}	3.87 ± 0.57	3.23 ± 0.45
THA	1.318×10^4	4.352×10^{-3}	1.65 ± 0.40	1.66 ± 0.61

[a]Measured in UW buffered by phosphate (pH = 6.7).
[b]H_2O_2 used as an actinometer.

We also examined the degradation of PABs by UV/H_2O_2 (0.1 mM). The degradation efficiencies of FLO, CAP and THA by UV/H_2O_2 were 78.99, 89.06 and 74.21% in UW for 30 min of reaction time (Fig. S7A) and were 91.88, 96.29 and 87.74% in SW for 150 min of reaction time (Fig. S7B), respectively. The degradation of PABs in UW and SW follows the pseudo-first-order kinetic law as well. The observed degradation rate constants (k_{obs}) of FLO, CAP and THA in UW via UV/H_2O_2 as compared to photolysis increased from 2.18×10^{-4} s^{-1} (via UV) to 8.99 ($\pm$ 1.21) $\times 10^{-4}$ s^{-1}, 3.87×10^{-4} s^{-1} (via UV) to 12.17 ($\pm$ 0.48) $\times 10^{-4}$ s^{-1} and 1.65×10^{-4} s^{-1} (via UV) to 7.55 ($\pm$ 0.15) $\times 10^{-4}$ s^{-1}, respectively (Fig. 1). The contribution of indirect photolysis via HO· radical in UV/H_2O_2 process was 76% for FLO, 67% for CAP and 78% for THA in UW. In contrast, the k_{obs} values of FLO, CAP and THA by UV/H_2O_2 were 2.70×10^{-4} s^{-1}, 3.55×10^{-4} s^{-1} and 2.23×10^{-4} s^{-1} in SW, which were 3 times lower than those in UW, respectively. Furthermore, the contribution of indirect photolysis via HO· radicals in UV/H_2O_2 process was significantly suppressed to 27% for FLO, 9% for CAP and 26% for THA in SW (the contribution of direct photolysis via UV increased to 73% for FLO, 91% for CAP and 74% for THA in SW). These results indicated that the constituents of SW had a significant negative impact on the indirect photolysis of PABs by UV/H_2O_2.

We found that the degradation rate followed this order of: CAP > FLO > THA in for both UV photolysis and UV/H_2O_2 process. The difference in the degradation efficiency is probably due to the different electron structures of PABs (Fig. S8). The red boxes specify the transitional regions of the electronic cloud densities between the lowest unoccupied molecular orbital (LUMO) and the highest occupied molecular orbital (HOMO) of PABs. The electronic cloud densities in CAP are more efficiently separated than those in FLO and THA. The separation of electronic cloud densities could enhance the polarity and redox reactivity of the molecule [23]. Thus, CAP is more likely to have a higher hydroxyl radical attack or direct photolysis.

3.2. Impact of constituents on PABs degradation by UV/H_2O_2

Before investigating the aqueous matrix impacts on the degradation of PABs, preliminary tests were conducted to analyze the effect of reagent (H_2O_2 and PABs) and discussed in Text S3. Although a higher H_2O_2 concentration (0.1–0.4 mM) could obtain higher k_{obs} (Fig. S9A), the corrosivity and toxicity of H_2O_2 should be considered [32,33]. Due to the limited reactive species in the UV/H_2O_2 system, the k_{obs} for all PABs gradually decreased with their increasing PABs concentration (1–5 μM) (Fig. S9B). Considering the concentration level of PABs in the aquatic environment and the limit for H_2O_2 in drinking water [34,35], the initial concentrations of PABs (1 μM) and H_2O_2 (0.1 mM) were selected in the following studies, unless otherwise stated.

3.2.1. Effect of fulvic acid

Fulvic acid (FA) is a representative for dissolved organic matter (DOM) in water treatment plant [36]. The influence of FA on PABs degradation was conducted for different FA concentration. The k_{obs} for FLO, CAP and THA decreased from 8.99×10^{-4} to 2.35×10^{-4} s^{-1}, 12.17×10^{-4} to 5.46×10^{-4} s^{-1} and 7.55×10^{-4} to 3.11×10^{-4} s^{-1}, respectively, with FA dosage increasing from 0 to 10 mg L^{-1} (Fig. 2A). The inhibitory effect of FA on PABs degradation could be mainly due to the following reasons: (i) FA exerted an inner filter effect on the photolysis of H_2O_2 and PABs (ε_{DOM} = 5.224 L g^{-1} cm^{-1} in this work), and (ii) FA acted as radical scavengers [37]. For FLO, the k_{obs} did not decrease monotonically and slightly increased when FA was increased from 2 to 5 mg L^{-1}. At an appropriate dose of FA (e.g., 5 mg

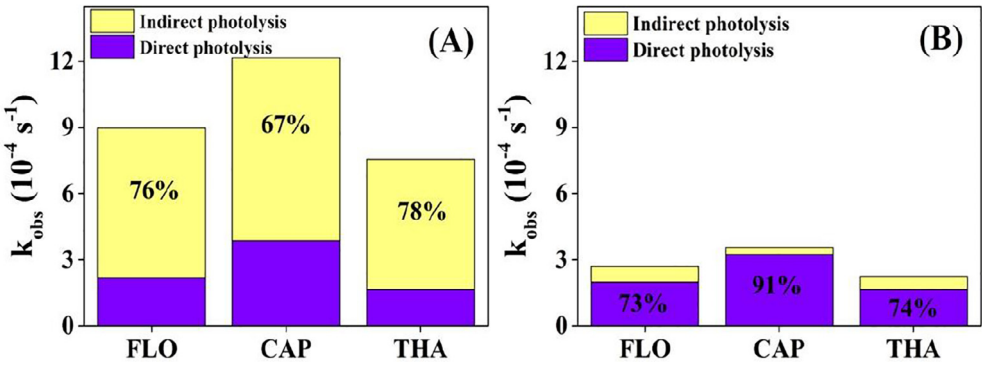

Fig. 1. The k_{obs} of PABs by UV/H_2O_2 in UW (A) and SW (B) (Conditions: $[PABs]_0$ = 1 μM, $[H_2O_2]$ = 0.1 mM, and $I_0 = 1.985 \times 10^{-6}$ E L^{-1} s^{-1}). Noting percentage represents the contribution of indirect and direct photolysis after individual k_{obs} normalization. Each column is representing 100% for each compound.

L^{-1} in this study), the oxidization effect of exited FA species on specific target pollutants (e.g., FLO) could exceed the scavenging effect of FA itself on radicals [38]. For CAP and THA, FA inhibited their degradation. Overall, FA has a negative effect on PABs degradation in UV/H_2O_2 process, especially at high concentrations of FA. Hence, pretreatment to eliminate FA may be required to achieve a satisfactory degradation of PABs in water using UV/H_2O_2 process.

3.2.2. Effect of alkalinity

At neutral pH, alkalinity of water is equal to the bicarbonates (HCO_3^-) concentration [39]. The effect of HCO_3^- (1–5 mM) on the PABs degradation is shown in Fig. 2B. The k_{obs} for FLO and THA gradually declined with increasing HCO_3^- concentration. In contrast, the k_{obs} for CAP sharply decreased by adding HCO_3^- (even as low as 1 mM) and then remained unchanged (from 1 mM to 5 mM). It was reported that HO· could react with HCO_3^-/CO_3^{2-} (HCO_3^- + HO· → $CO_3^{\cdot -}$ + H_2O, $k = 8.5 \times 10^6$ $M^{-1}{\cdot}s^{-1}$; CO_3^{2-} + HO· → $CO_3^{\cdot -}$ + OH^-, $k = 3.9 \times 10^8$ $M^{-1}{\cdot}s^{-1}$) to form $CO_3^{\cdot -}$ with low oxidation capacity (E^0 = ($CO_3^{\cdot -}$/CO_3^{2-} = 1.63 V at pH 8.4)) and high selectivity [40]. To a certain degree, the $CO_3^{\cdot -}$ produced might compensate for the loss of HO· needed for CAP degradation [41]. Nevertheless, the presence of HCO_3^- had negative effect on the degradation of PABs during UV/H_2O_2 process.

3.2.3. Effect of chloride

As shown in Fig. 2C, the chloride (Cl^-) had virtually no impact on PABs degradation using UV/H_2O_2 process. Although there is a reaction between HO· and Cl^- (Cl^- + HO· → $ClHO^{\cdot -}$, $k = 4.3 \times 10^9$ $M^{-1}{\cdot}s^{-1}$), there is also a rapidly reversible reaction ($ClHO^{\cdot -}$ → Cl^- + HO·, $k = 6.1 \times 10^9{\cdot}s^{-1}$) [42–44], which maintains a stable HO· concentration in solution.

3.2.4. Effect of nitrate

The redox potential of $NO_3{\cdot}/NO_3^-$ is almost comparable to HO·/H_2O [45]. It has been reported that nitrate (NO_3^-) could enhance the photodegradation of contaminants [25,46,47] because it can produce HO· under either UV or sunlight exposure [48,49]. In this system, the

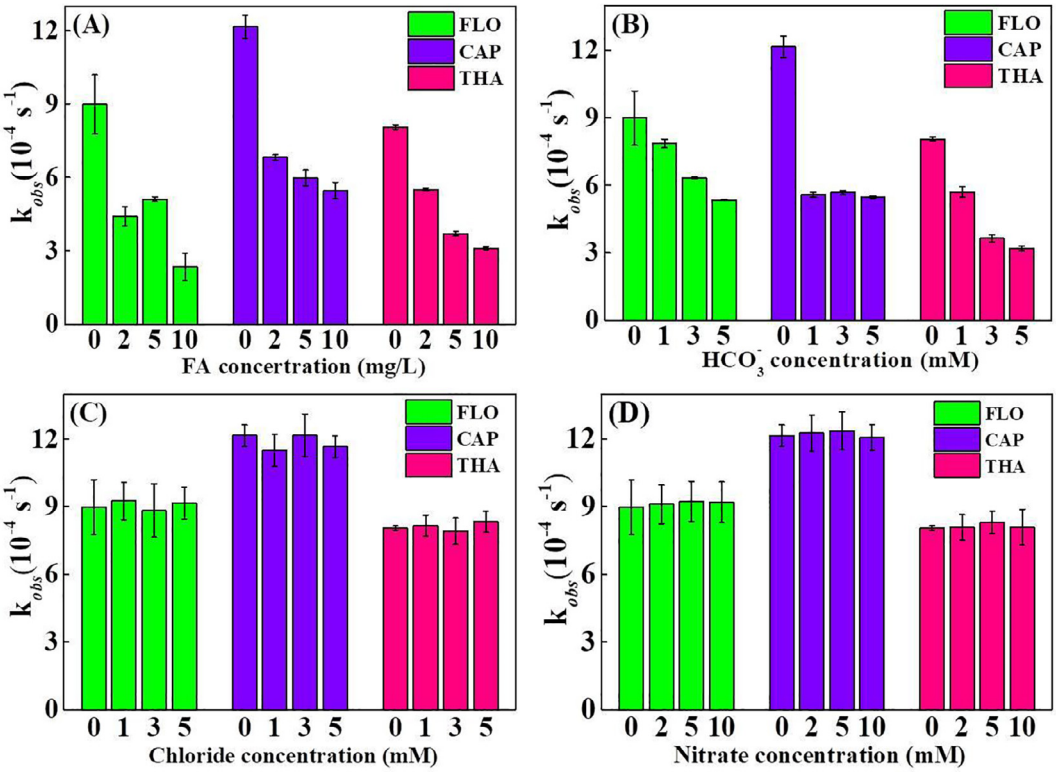

Fig. 2. Effect of FA (A), HCO_3^- (B), chloride (C) and nitrate (D) on the degradation kinetics of PABs by UV/H_2O_2 (Conditions: $[PABs]_0$ = 1 μM, $[H_2O_2]$ = 0.1 mM, t = 30 min, and $I_0 = 1.985 \times 10^{-6}$ E L^{-1} s^{-1}).

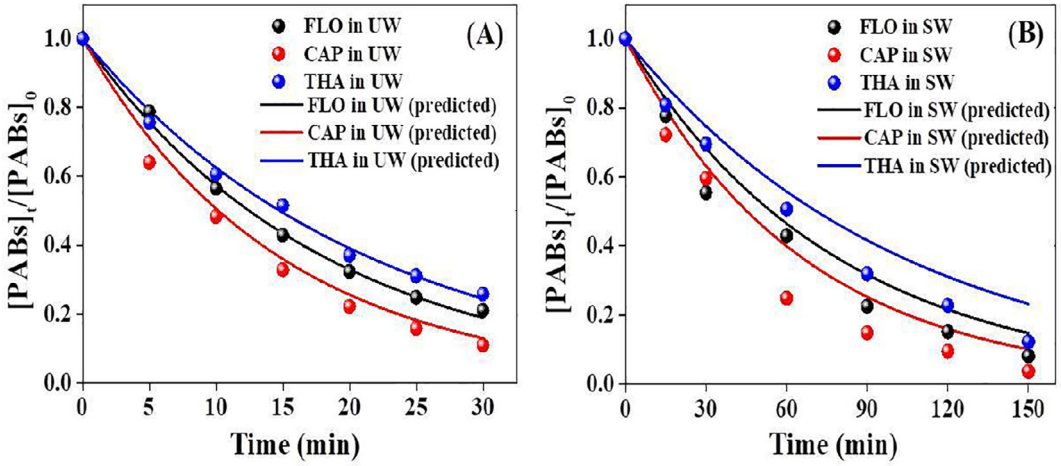

Fig. 3. Degradation of PABs in UW (A) and SW (B) by UV/H_2O_2. The symbols represent experimental data and lines represent model predictions (Conditions: $[PABs]_0$ = 1 μM, $[H_2O_2]$ = 0.1 mM, and $I_0 = 1.985 \times 10^{-6}$ E L^{-1} s^{-1}).

pseudo-steady state concentration of HO· generated by NO_3^- (i.e., 10 mM) was calculated to be 2.94×10^{-16} M for FLO, 2.87×10^{-16} M for CAP and 2.99×10^{-16} M for THA by method described in previous research [47]. However, the quantity of HO· produced from NO_3^- is not sufficient for observable degradation for the PABs, due to the low quantum yield (Φ_{NO3^-} = 0.0017 mol/Einstein) and low absorbance of NO_3^- (Fig. S10). As a result, NO_3^- did not show an obvious impact on PABs degradation (Fig. 2D).

3.3. Mathematical modeling of UV/H_2O_2 process

A mathematical model was used to predict PABs degradation based on the simplified pseudo-steady-state hypothesis. The overall degradation by both direct photolysis and indirect photolysis can be described by Eq. (5):

$$\frac{d[PABs]}{dt} = k_{obs}[PABs] = (k_d + k_i)[PABs] \quad (5)$$

where k_d (s^{-1}) and k_i (s^{-1}) are the pseudo-first-order rate constant of direct photolysis and indirect photolysis, respectively. According to the obtained Φ_{254nm} and ε_{254nm} of PABs (Table 1), as well as I_0 and b of the photoreactor (Figs. S3 and S4), k_d can be described by Eqs. (6) and (7) [50].

$$\frac{d[PABs]}{dt} = \Phi_{254nm} I_0 F_{s254nm} F_{H254nm} = k_d[PABs] \quad (6)$$

$$k_d = \frac{\Phi_{254nm} I_0 F_{s254nm} F_{H254nm}}{[PABs]} \quad (7)$$

where F_{s254nm} and F_{H254nm} are the fraction of light absorbed by solution and PABs, respectively. They can be expressed as:

$$F_{s254nm} = 1 - 10^{-(\alpha_{254nm} + \varepsilon_{254nm}[PABs])b} \quad (8)$$

$$F_{H254nm} = \frac{\varepsilon_{254nm}[PABs]}{\varepsilon_{254nm}[PABs] + \alpha_{254nm}} \quad (9)$$

α_{254nm} (cm^{-1}) is the absorption coefficient of the solvent (using deionized water as a blank).

The indirect photolysis rate (k_i) can be expressed as a function of the second-order rate constant of PABs reacting with HO· ($k_{HO\cdot,PABs}$) and the steady-state concentration of HO· ($[HO\cdot]_{ss}$) [15,24,51]:

$$k_i = k_{HO\cdot,PABs}[HO\bullet]_{ss} \quad (10)$$

3.3.1. Determination of $k_{HO\cdot,\ PABs}$

A competition kinetic method was employed to determine the second-order rate constants $k_{HO\cdot,PABs}$ between PABs and HO· (Text S4). *p*-chlorobenzoic acid (*p*CBA) was used as the competitor because it essentially does not undergo direct photolysis under typical UV/H_2O_2 conditions [40]. The reactions of HO· with individual PAB and *p*CBA are assumed to proceed independently and in parallel. In competition kinetic experiments, the $k_{HO\cdot,PABs}$ values of PABs with HO· are (3.94 ± 0.73) $\times 10^9$ $M^{-1}s^{-1}$, (4.85 ± 0.45) $\times 10^9$ $M^{-1}s^{-1}$ and (3.37 ± 0.68) $\times 10^9$ M^{-1} s^{-1} for FLO, CAP and THA, respectively. In general, the reaction rate constants of organics with HO· vary from 10^6 to 10^{10} M^{-1} s^{-1} [30], indicating that the reaction rates between PABs and HO· are very rapid.

3.3.2. Estimation of $[HO\cdot]_{ss}$

The steady-state concentration of HO· was estimated by a simplified pseudo-steady state model. The HO· concentration is assumed to be constant over the reaction period. It can be calculated as the ratio of produced to consumed HO· by Eq. (11).

$$[HO\bullet]_{ss} = \frac{2\Phi_{H_2O_2} I_0 f_{H_2O_2}(1-10^{-A})}{\sum k_{HO\bullet,s} C_s} \quad (11)$$

where Φ_{H2O2} is the quantum yield from the photolysis of H_2O_2, f_{H2O2} is the fraction of light absorbance from H_2O_2, A is the total light absorbance from solution components, $k_{HO\cdot,s}$ (M^{-1} s^{-1}) is the second-order rate constant of scavenger reacting with HO·, and C_s (M) is scavenger concentration. The scavenging effects by PABs, H_2O_2 and cosolutes are expressed by the concentration of individual scavengers, multiplied by their second-order rate constants with HO· (Table S4). The concentrations of these compounds are assumed to be constant during reaction. The measured $k_{HO\cdot,PABs}$ and the estimated $[HO\cdot]_{ss}$ were used in Eq. (10) to determine the first-order rate constant k_i of PABs. Then, combining the k_i and k_d into Eq. (5), the predicted degradation of FLO, CAP and THA by UV/H_2O_2 in UW and SW were obtained and shown in Fig. 3.

The proposed pseudo-steady-state kinetic model agrees well with the experimental data for all PABs in UW (Fig. 3A). In comparison, the predicted degradation efficiencies of PABs in SW were underestimated (Fig. 3B). This is mainly due to the modeling assumed matrix constituent concentrations remaining constant during the UV/H_2O_2 process. In fact, scavengers should gradually decrease with reaction process, and their negative impact became weak. Therefore, the predicted residual concentrations of PABs were higher than measured concentrations.

3.4. Transformation pathway and proposed reaction mechanism

The degradation products of PABs via UV/H_2O_2 were measured using LC/MS. The extraction ion chromatogram (EIC) for the detection of these products is shown in Figs. S11–S13. Five major byproducts of FLO (FLO-TPs) with the *m/z* of 276, 336, 338, 354 and 372 were observed (Fig. S11). Mass deviations of the proposed formulas are in the range of ± 10 ppm except for TP-276 (12.7 ppm) (Table S5). The 16 Da addition of TP-372–1,2 (*m/z* 372, $C_{12}H_{13}Cl_2FNO_5S$) to the molecular weight of parent compound FLO (*m/z* 356) suggested a transformation pathway of hydroxylation. TP-372-1,2 was likely produced by the direct addition of HO· to the benzene moiety, but the definite position of the hydroxyl group was uncertain. The 2 Da reduction for FLO (TP-354, *m/z* 354, $C_{12}H_{11}Cl_2FNO_4S$) implies a hydrogen abstraction reaction forming double bonds.

HO· is a strong electrophile and attacks organic compounds via hydrogen abstraction, addition and electron transfer. On the one hand, HO· radicals attack benzene rings in PABs to generate hydroxycyclohexadienyl (HCD) radicals, which can be stabilized by resonance; on the other hand, the benzene rings in PABs can produce benzene radical cations via electron transfer, which further react with water to form HCD radicals (Scheme S1) [16,52]. The produced HCD radicals further react with oxygen to form peroxy radicals (C-OO·) [16] and then form a hydroxylated product (TP-372-1,2 for FLO). It is noted that the formation of multiple hydroxyl products was not observed. This is mainly attributed to the existence of a steric hindrance effect of $–SO_2CH_3$ group and bulky para groups. In addition, the existence of peroxide radicals in hydroxyl-containing organic compounds can transform ketone, alcohol, aldehyde and carboxylic acid compounds [53]. For FLO, the carbonyl product of TP-354 was observed through the loss of a HO_2·. TP-338 (*m/z* 338, $C_{12}H_{14}ClFNO_5S$) and TP-336 (*m/z* 336, $C_{12}H_{12}ClFNO_5S$) are the dehalogenation products from FLO itself and TP-354, respectively, likely due to the nucleophilic substitution reactions. The following elimination of $–SO_2CH_3$ from the side of TP-354 can form TP-276 (*m/z* 276, $C_{11}H_9Cl_2FNO_2$). Li proposed that main transformation pathways via HO· of FLO were involved in hydroxylation, oxygenation, and dehydrogenation [54]. Because standards of the byproducts are not commercially available, the accurate quantification of each byproduct is impossible to achieve. The abundance of byproducts was evaluated by peak area (Fig. S14A). On the basis of the structures proposed for major byproducts, a transformation pathway for FLO is proposed in Fig. 4.

The products of TP-337-1,2 (*m/z* 337, $C_{11}H_{11}Cl_2N_2O_6$) for CAP (Fig. S12) and TP-370-1,2 (*m/z* 370, $C_{12}H_{14}Cl_2NO_5S$) for THA (Fig. S13) are hydroxylated. Their formation pathway is similar to TP-372–1,2 for FLO (Scheme S1). Other intermediates (TP-152 and TP-187 for CAP in Fig. S12; TP-220 and TP-390 for THA in Fig. S13) were also observed. However, their structures were not identified according to the current information. The variations of byproducts for CAP and THA after different reaction time were shown in Figs. S14B and S14C, respectively. The intermediates generated from PABs via UV/H_2O_2 were still present at the end of reaction. The results likely indicate that these intermediates were poorly mineralized and might have biological reactivity. Therefore, it is necessary to evaluate their toxicity and TCMFP for post-chlorine treatment.

3.5. Toxicity evaluation

3.5.1. Antimicrobial property

As a representative of microorganisms in aquatic environments, *Escherichia coli* is commonly used to test the antimicrobial property of PABs and their byproducts [13,55]. The inhibition was calculated according to Eq. (12):

$$\text{Inhibiton}(\%) = \left(1 - \frac{OD_{600}(s)}{OD_{600}(c)} \times 100\%\right) \quad (12)$$

where OD_{600} (s) was the absorbance at 600 nm of the sample taken at each selected time interval, and OD_{600} (c) was the absorbance of the control.

Because standards of byproducts are not commercially available, it is difficult to separately test the toxicity of the products. Despite this, it is highly valuable to test the inhibition effect of a mixture of byproducts and residual parent compounds. The observed inhibition of the samples was shown in Fig. 5A. The antimicrobial activity of PABs gradually decreased via UV/H_2O_2 with prolonged treatment time. The inhibition efficiencies decreased to 14.50% for THA, 16.96% for FLO and 17.13% for CAP after 30 min of the UV/H_2O_2 treatment. Meanwhile, inhibition rate of byproducts generated could be calculated through subtracting the corresponding inhibition of the residual antibiotic concentration from samples. Obviously, the inhibition proportion of residual antibiotic occupied the dominant part even at the end of reaction (Fig. 5A), which indicated that byproducts formed has low antibacterial activity.

The byproducts of PABs via UV/H_2O_2 have obviously lower antimicrobial activity towards *Escherichia coli* bacterium. PABs can cross-link with the 50S subunit of 70S ribosome in *Escherichia coli* at the entrance to the ribosomal peptide exit tunnel, leading to interference with protein biosynthesis [56]. After treatment by UV/H_2O_2, the ability of PABs byproducts to bind the subunits is probably less than that of their parent compounds. Thus, the ribosome could more efficiently participate in protein synthesis.

3.5.2. Acute toxicity

The marine bacterium *Vibrio fischeri* is commonly used as an indicator of acute toxicity [57,58]. The bioluminescence of *Vibrio fischeri* will decrease in the presence of toxic compounds via the interference on normal metabolism.

Fig. 5B exhibits the acute toxicity evolution of PABs after the UV/H_2O_2 treatment. The luminescence (L) variance of *Vibrio fischeri* in the PABs solution with different UV/H_2O_2 treatment time (t) reflects the variation of acute toxicity. The data points above the dashed line (representing no change in the luminescence) indicate the decline of toxicity with increased luminescence. Likewise, the data points below the dashed line indicate the increase of toxicity with lower luminescence. Significantly, the acute toxicity of FLO and THA samples increased throughout the UV/H_2O_2 treatment. In contrast, the acute toxicity of the CAP samples decreased after 30 min of the UV/H_2O_2 treatment.

Bacterial luciferase can oxidize riboflavin 5′-phosphate ($FMNH_2$) to FMN [59]. In addition, $FMNH_2$ is necessary for *Vibrio fischeri* to exhibit bioluminescence activity [60]. Hydroxylated compounds are prone to combine with $FMNH_2$ through hydrogen to block the bonding between $FMNH_2$ and luciferase in *Vibrio - qinghaiensis* sp.-Q67 [61]. Higher acute toxicity could result from the hydroxylated byproducts in the FLO and THA samples. Although the antimicrobial activity of PABs toward *Escherichia coli* was reduced, the acute toxicity of FLO and THA towards *Vibrio fischeri* increased after the UV/H_2O_2 treatment. Hence, a single bioassay was insufficient to comprehensively evaluate the toxicity of the byproducts.

3.5.3. Ecotoxicity

QSAR analysis was used to predict the ecotoxicity of PABs and byproducts using the ECOSAR program. The prediction of the ECOSAR program is based on the definite chemical structures of target pollutants. Because the chemical structures of byproducts of CAP and THA were not accurately identified, ecotoxicity calculations were only performed for FLO and its byproducts. The EC_{50} values represent the half effective concentration, and LC_{50} values represent the half lethal concentration. The Chronic Value (ChV) represents chronic toxicity and is defined as the geometric mean of the no observed effect concentration and the lowest observed effect concentration. The toxicities for fish, daphnid and green algae were calculated and the results are shown in Table 2. Green algae were the species most sensitive to FLO and its

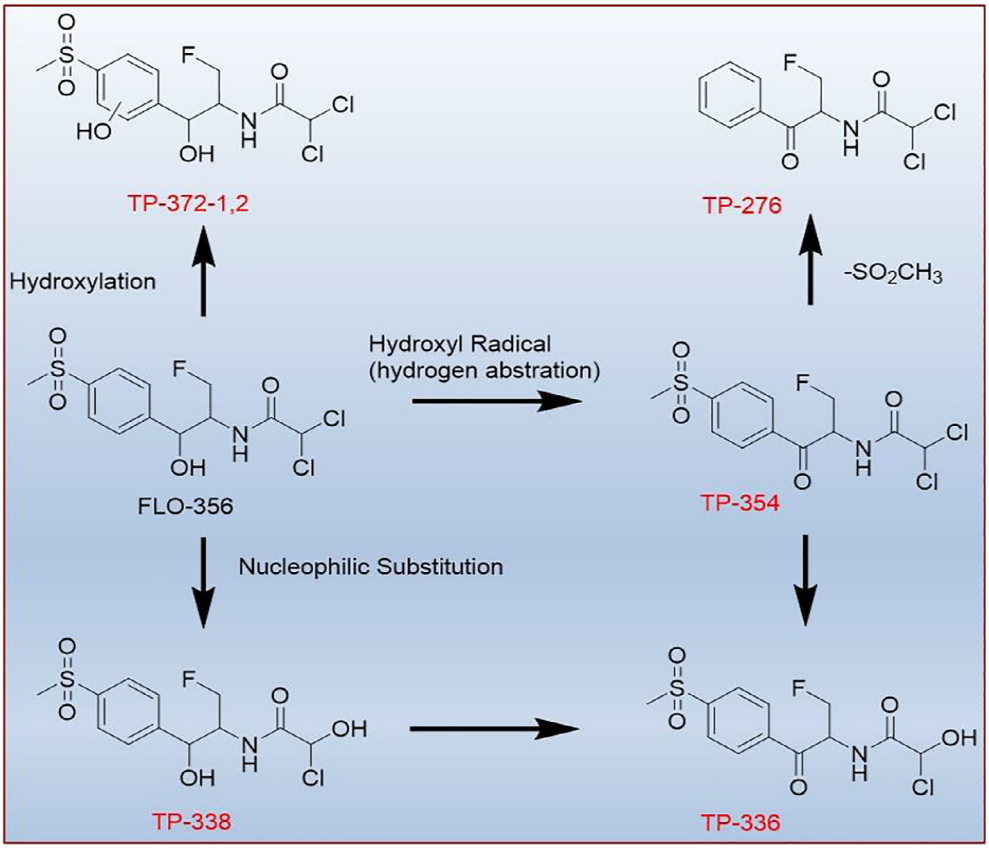

Fig. 4. Proposed structures of byproducts and degradation pathways on FLO under UV/H_2O_2.

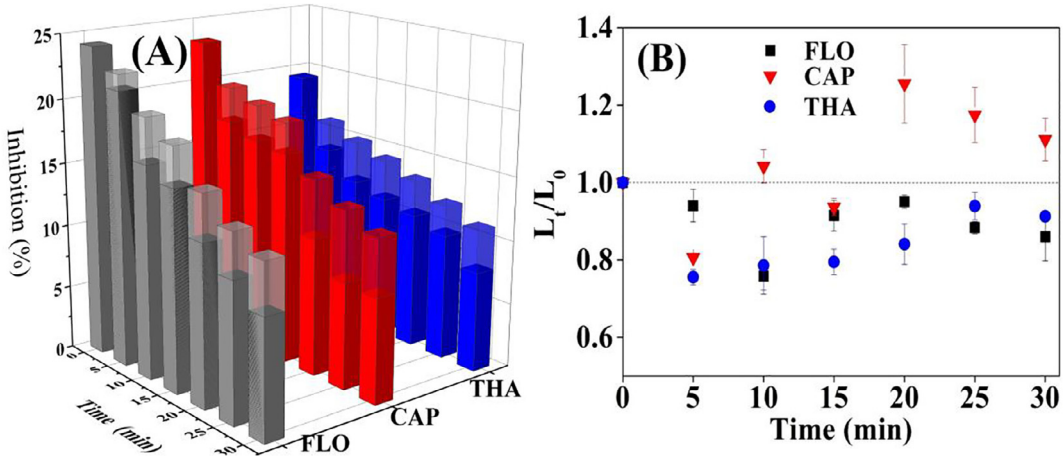

Fig. 5. Inhibition on *Escherichia coli* (A) and *Vibrio fischeri* luminescence (B) by the samples in UW after different UV/H_2O_2 treatment time (Conditions: $[PABs]_0 = 1\ \mu M$, $[H_2O_2] = 0.1$ mM, and $I_0 = 1.985 \times 10^{-6}$ E L^{-1} s^{-1}). Noted the upper transparency moiety (A) displayed the inhibition resulting from the byproducts generated.

byproducts. Meanwhile, TP-276 and TP-354 of FLO exhibited much higher toxicity than FLO for fish, daphnid and green alage. In terms of chronic toxicity for daphnid and green alage, the difference between species was increased compared to the results of acute toxicity.

3.6. TCMFP by Post-Chlorination treatment

Chlorine is a strong oxidative disinfectant and can react with aromatic compounds quickly by electrophilic substitution [62]. PABs can discharge into drinking water sources and react with the chlorine to generate carbonaceous/nitrogens-containing disinfection byproducts (C/N-DBPs) [22,63,64]. Generally, TCM is one of the final byproducts after the chlorination of drinking water, and TCM has high stability in the presence of chlorine. The yields of TCM after 24 h chlorination of FLO, CAP and THA in UW and SW without pre-oxidation were 0.19 and 35.71, 0.17 and 37.74, 0.32 and 38.69%, respectively (Fig. 6). The significant enhanced TCM yield for PABs in SW was attributed to FA, which react with chlorine resulting in more TCM formation. All the PABs showed similar TCM yield for chlorination in UW or SW, which is likely due to the similar molecular structure of the PABs (Table S1).

In UW, after 30 min pretreatment with UV alone, the TCM yields for FLO, CAP and THA during the subsequent chlorination were up to 0.38%, 0.37% and 0.33%, respectively. And it was 2.0, 2.2 and 1.8 times higher than those without pre-oxidation, respectively. Likewise,

Table 2
Ecotoxicity of FLO and byproducts for fish, daphnid and green algae.[a]

Compound	Acute toxicity			Chronic toxicity		
	Fish (96-h LC_{50})	Daphnid (48-h LC_{50})	Green algae (96-h EC_{50})	Fish (ChV)	Daphnid (ChV)	Green algae (ChV)
TP-276	5.43	14.44	0.02	1.47	4.90	0.01
TP-354	43.37	80.31	0.45	17.32	53.31	0.25
FLO	145.62	212.48	2.69	75.01	219.36	2.58
TP-372-1,2	281.26	363.43	6.97	164.91	469.91	8.91
TP-336	551.80	611.54	19.81	381.11	1050.86	36.46
TP-338	1101.82	1066.29	54.84	879.34	2355.42	139.24

[a] Unit = $mg{\cdot}L^{-1}$.

the TCM yield for PABs in SW was further elevated after 30 min pretreatment with UV alone. Prolonging UV irradiation (e.g., 60 min and 90 min) can hardly change the TCM yields for all PABs in UW and SW, and it can be even increased to some extent (Fig. 6). In addition, DOC evolution for PABs via UV alone in UW and SW were not evidently reduced within 90 min (Fig. 7). These results indicated UV alone pretreatment subsequent chlorination could hardly reduce the TCM yield.

Surprisingly, after 30 min UV/H_2O_2 pretreatment, the TCM yields for FLO, CAP and THA in UW during subsequent chlorination increased up to 0.47%, 0.41% and 0.39%, which are 2.5, 2.4 and 2.2 times higher than those without the pre-oxidation, and exceed those with UV pretreatment. Noteworthy, when further increasing the irradiation time using UV/H_2O_2 pretreatment (e.g., 60 min and 90 min), the TCM yield for PABs significantly reduced. This is mainly due to the corresponding DOC diminution (Fig. 7). The results implied extending irradiation using UV/H_2O_2 can effectively decrease the TCM yield for all PABs. Interestingly, in SW, after 30 min UV/H_2O_2 pretreatment, the TCM yields for FLO, CAP and THA during subsequent chlorination decreased to 0.98%, 0.57% and 0.97%, which are 36, 66 and 40 times lower than those without the pre-oxidation process. This phenomenon implicates that UV/H_2O_2 process could appropriate to reduce TCM yields in SW, which is mainly due to the DOC mineralization by HO· generated (Fig. 7). And the TCM yield for FLO and CAP hardly changed when prolonging the UV/H_2O_2 pretreatment up to 90 min, yet for THA gradually reduced.

Direct UV photolysis could destroy PABs, but H_2O_2 in the presence of UV irradiation would be much more powerful because HO· was produced. The generated products of PABs via UV and UV/H_2O_2 pretreatment with 30 min appeared to be more readily substituted to further form TCM than PABs itself (Fig. 6). Similarly, UV/persulfate (UV/PS) or UV pretreatment for CAP followed by chlorination could also significantly increase TCM production [65]. However, further lengthening time for UV/H_2O_2 process will decrease TCMFP attributing to HO· oxidation ability for the generated byproducts. As for SW, UV alone could upgrade the TCM yields and UV/H_2O_2 process greatly diminishes them. Therefore, the TCMFP can be dramatically addressed in UW and SW when prolonging time of UV/H_2O_2 process.

3.7. Reaction in real water matrices

The reaction efficiency was further assessed using real water matrices with the aim of examining the possible reaction under natural water matrices (Xiangjiang River and Taozi Lake). Meanwhile, general characteristics of real water matrices were shown in Table S6. These samples were spiked with 1 μM of PABs and 100 μM of H_2O_2. As shown in Fig. 8, the samples from Xiangjiang River and Taozi Lake with dissolved organic matter (DOM) content (DOC, UV_{254}) and alkalinity exhibited lower removal efficiency than that in UW. The existence of FA and HCO_3^- could inhibit the PABs oxidation with UV/H_2O_2 process (Fig. 2). CAP exhibited as well the fastest degradation rates in real water matrices. Hence, PABs removal by UV/H_2O_2 process in real water must take into account the natural organic matter and alkalinity.

4. Conclusions

This study comprehensively evaluated the UV/H_2O_2 process for the degradation of PABs. The interference of constituents in water matrixes on PABs degradation was thoroughly investigated. Pseudo-steady-state kinetic model successfully predicted the impact of water constituents on PABs degradation. The transformation of PABs was triggered via

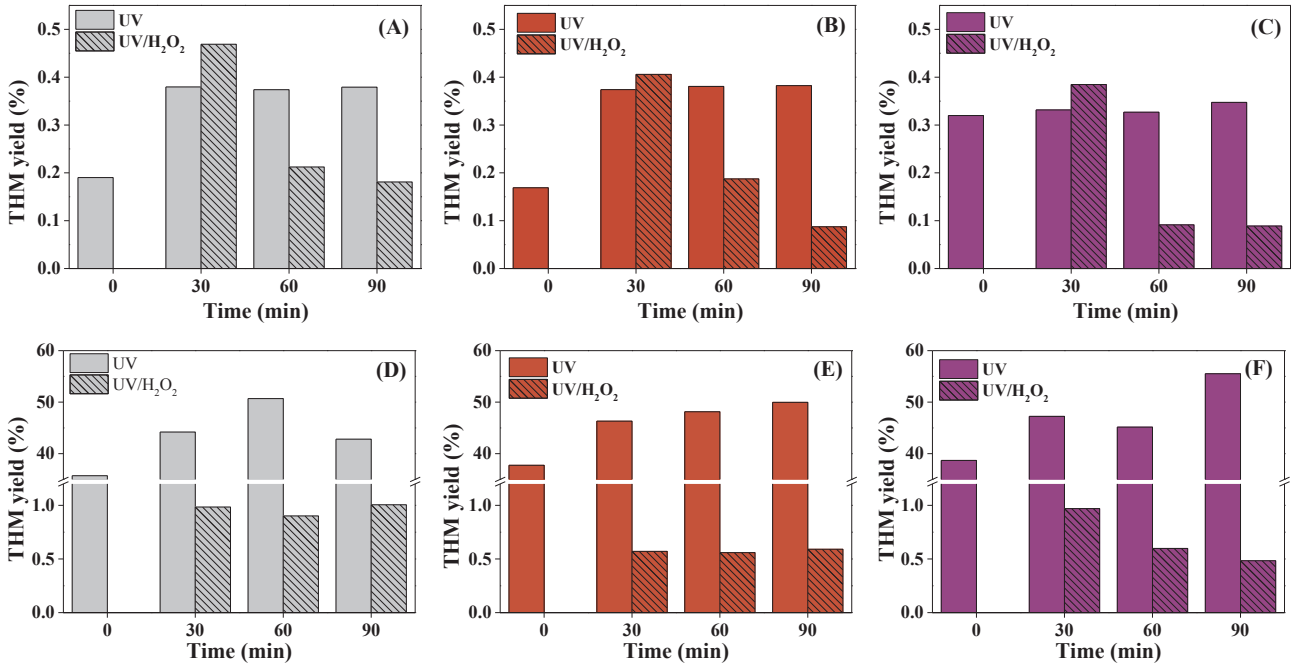

Fig. 6. TCM yield of FLO (A and D), CAP (B and E) and THA (C and F) in UW (up) and SW (down) without or with UV alone as well as UV/H_2O_2 pretreatment subsequent chlorination (Conditions: $[PABs]_0$ = 3 μM, Cl_2 dose = 1.0 mM, and $[H_2O_2]$ = 0.3 mM).

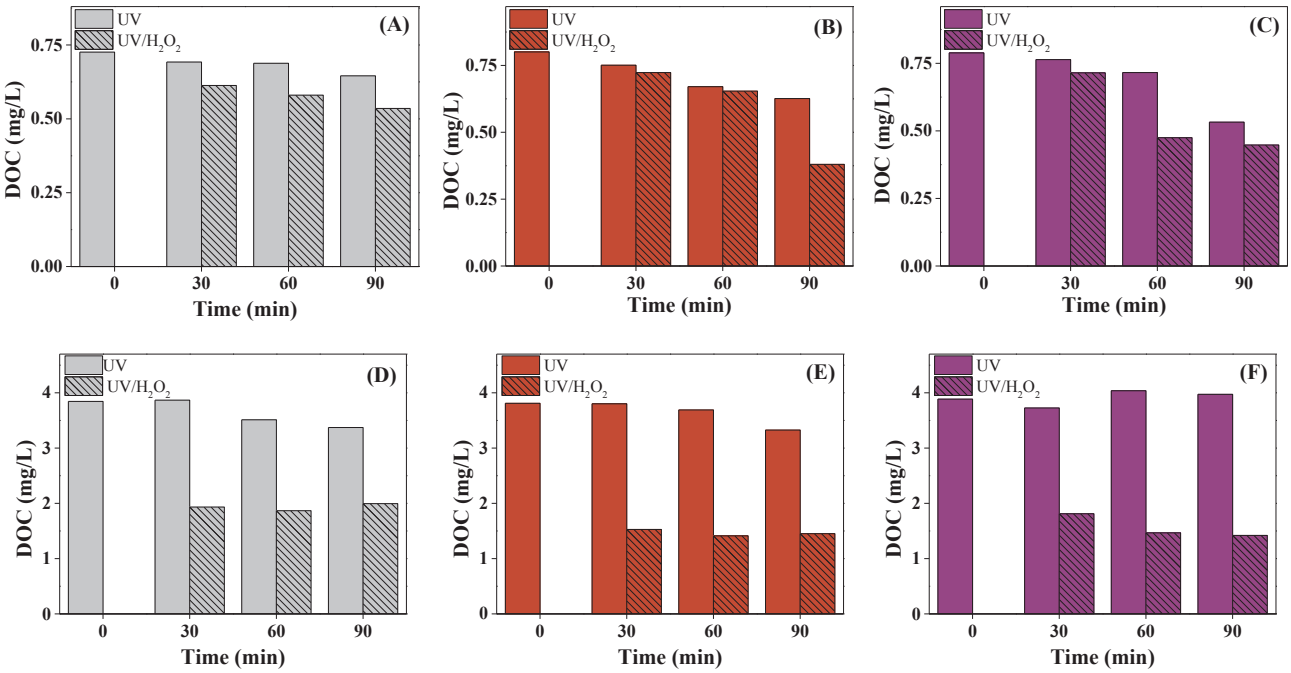

Fig. 7. DOC evolution of FLO (A and D), CAP (B and E) and THA (C and F) in UW (up) and SW (down) without or with UV alone as well as UV/H_2O_2 pretreatment subsequent chlorination (Conditions: $[PABs]_0$ = 3 μM, Cl_2 dose = 1.0 mM, and $[H_2O_2]$ = 0.3 mM).

hydroxylation and/or hydrogen abstraction. DFT calculations confirm that the separation of the electron cloud densities of PAB molecules was favorable to hydroxyl radical attack or direct photolysis via the UV/H_2O_2 process. The antimicrobial property, acute toxicity and ecotoxicity of PABs and their byproducts via the UV/H_2O_2 process were comprehensively evaluated for the first time. It is noted that the acute toxicity of FLO and THA after UV/H_2O_2 treatment increased, and two identified byproducts of FLO exhibited higher ecotoxicity than FLO itself. Furthermore, after 30 min UV or UV/H_2O_2 pretreatment in UW, the TCMFP significantly increased in post-chlorination. However, when prolonging the UV/H_2O_2 pretreatment up to 90 min, the TCM yield for PABs substantially reduced. This may due to the corresponding DOC diminution. As for SW, the TCM yields were promoted by UV alone pretreatment, while significantly reduced by UV/H_2O_2 pretreatment due to the DOC mineralization by HO· generated. Besides, PABs removal was subjected to natural organic matter and alkalinity in real water matrices. Overall, this study achieves a better understanding on UV/H_2O_2 process for PABs degradation. Additionally, to comprehensively evaluate the performance of UV-based AOPs for destroying contaminants, future research should be conducted to evaluate other matrices (e.g., seawater and urine) to minimize the knowledge gaps of various aqueous environment.

Acknowledgments

This work was supported by the National Natural Science Foundation of China (51478171, and 51778218). The authors appreciate the support from the Brook Byers Institute for Sustainable Systems, Hightower Chair and Georgia Research Alliance at the Georgia Institute of Technology. The views and ideas expressed herein are solely those of the authors and do not represent the ideas of the funding agencies in any form. And we do thank the English editing by ChemWorx.

Appendix A. Supplementary data

Supplementary data associated with this article can be found, in the online version, at http://dx.doi.org/10.1016/j.cej.2018.06.164.

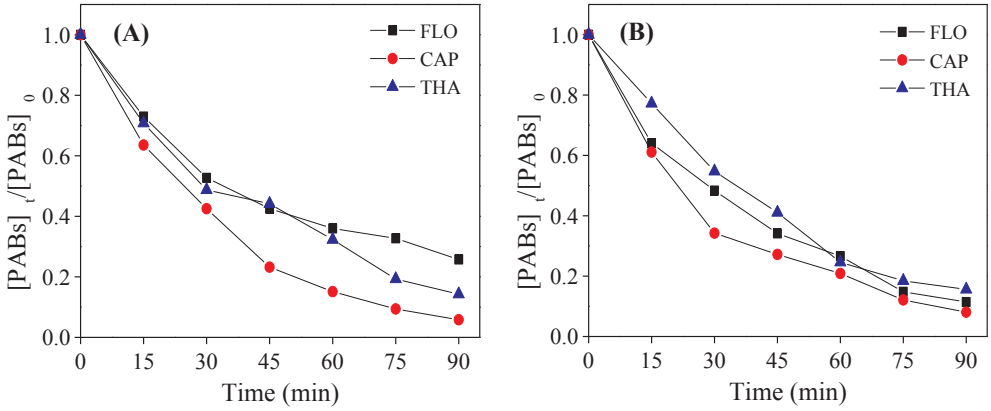

Fig. 8. The oxidation kinetics of PABs by UV/H_2O_2 in Xiangjiang (A) and Taozi Lake (B). (Conditions: $[PABs]_0$ = 1 μM, $[H_2O_2]$ = 0.1 mM, and $I_0 = 1.985 \times 10^{-6}$ E L^{-1} s^{-1}).

References

[1] C. Carlsson, A.K. Johansson, G. Alvan, K. Bergman, T. Kühler, Are pharmaceuticals potent environmental pollutants? Part I: environmental risk assessments of selected active pharmaceutical ingredients, Sci. Total Environ. 364 (2006) 67–87.

[2] A. Sapkota, A.R. Sapkota, M. Kucharski, J. Burke, S. McKenzie, P. Walker, R. Lawrence, Aquaculture practices and potential human health risks: current knowledge and future priorities, Environ. Int. 34 (2008) 1215–1226.

[3] J. Li, B. Shao, J.Z. Shen, S.C. Wang, Y.N. Wu, Occurrence of chloramphenicol-resistance genes as environmental pollutants from swine feedlots, Environ. Sci. Technol. 47 (2013) 2892–2897.

[4] S. Rodriguez-Mozaz, S. Chamorro, E. Marti, B. Huerta, M. Gros, A. Sànchez-Melsió, C.M. Borrego, D. Barceló, J.L. Balcázar, Occurrence of antibiotics and antibiotic resistance genes in hospital and urban wastewaters and their impact on the receiving river, Water Res. 69 (2015) 234–242.

[5] Q.Q. Zhang, A. Jia, Y. Wan, H. Liu, K.P. Wang, H. Peng, Z.M. Dong, J.Y. Hu, Occurrences of three classes of antibiotics in a natural river basin: association with antibiotic-resistant Escherichia coli, Environ. Sci. Technol. 48 (2014) 14317–14325.

[6] K. Choi, Y. Kim, J. Jung, M.H. Kim, C.S. Kim, N.H. Kim, J. Park, Occurrences and ecological risks of roxithromycin, trimethoprim, and chloramphenicol in the Han River, Korea, Environ. Toxicol. Chem. 27 (2008) 711–719.

[7] S.D. Richardson, T.A. Ternes, Water analysis: emerging contaminants and current issues, Anal. Chem. 83 (2011) 4614–4648.

[8] D.Y. Kong, B. Liang, D.-J. Lee, A.J. Wang, N.Q. Ren, Effect of temperature switchover on the degradation of antibiotic chloramphenicol by biocathode bioelectrochemical system, J. Environ. Sci. 26 (2014) 1689–1697.

[9] M.I. Badawy, R.A. Wahaab, A. El-Kalliny, Fenton-biological treatment processes for the removal of some pharmaceuticals from industrial wastewater, J. Hazard. Mater. 167 (2009) 567–574.

[10] X.Z. Peng, Z.D. Wang, W.X. Kuang, J.H. Tan, K. Li, A preliminary study on the occurrence and behavior of sulfonamides, ofloxacin and chloramphenicol antimicrobials in wastewaters of two sewage treatment plants in Guangzhou, China, Sci. Total Environ. 371 (2006) 314–322.

[11] L.J. Zhou, G.G. Ying, S. Liu, J.L. Zhao, B. Yang, Z.F. Chen, H.J. Lai, Occurrence and fate of eleven classes of antibiotics in two typical wastewater treatment plants in South China, Sci. Total Environ. 452 (2013) 365–376.

[12] C. Baeza, D.R. Knappe, Transformation kinetics of biochemically active compounds in low-pressure UV photolysis and UV/H_2O_2 advanced oxidation processes, Water Res. 45 (2011) 4531–4543.

[13] O.S. Keen, K.G. Linden, Degradation of antibiotic activity during UV/H_2O_2 advanced oxidation and photolysis in wastewater effluent, Environ. Sci. Technol. 47 (2013) 13020–13030.

[14] B. Wols, C. Hofman-Caris, D. Harmsen, E. Beerendonk, Degradation of 40 selected pharmaceuticals by UV/H_2O_2, Water Res. 47 (2013) 5876–5888.

[15] H. Yao, P.Z. Sun, D. Minakata, J.C. Crittenden, C.-H. Huang, Kinetics and modeling of degradation of ionophore antibiotics by UV and UV/H_2O_2, Environ. Sci. Technol. 47 (2013) 4581–4589.

[16] R.C. Zhang, Y.K. Yang, C.H. Huang, N. Li, H. Liu, L. Zhao, P.Z. Sun, UV/H_2O_2 and UV/PDS treatment of trimethoprim and sulfamethoxazole in synthetic human urine: transformation products and toxicity, Environ. Sci. Technol. 50 (2016) 2573–2583.

[17] M.C. Dodd, H.P.E. Kohler, U.V. Gunten, Oxidation of antibacterial compounds by ozone and hydroxyl radical: elimination of biological activity during aqueous ozonation processes, Environ. Sci. Technol. 43 (2009) 2498–2504.

[18] D. Fatta-Kassinos, M. Vasquez, K. Kümmerer, Transformation products of pharmaceuticals in surface waters and wastewater formed during photolysis and advanced oxidation processes–degradation, elucidation of byproducts and assessment of their biological potency, Chemosphere 85 (2011) 693–709.

[19] M. Molkenthin, T. Olmez-Hanci, M.R. Jekel, I. Arslan-Alaton, Photo-Fenton-like treatment of BPA: effect of UV light source and water matrix on toxicity and transformation products, Water Res. 47 (2013) 5052–5064.

[20] L.B. Stadler, A.S. Ernstoff, D.S. Aga, N.G. Love, Micropollutant fate in wastewater treatment: redefining "removal", Environ. Sci. Technol. 46 (2012) 10485–10486.

[21] Y.M. Zhang, W.H. Chu, T. Xu, D.Q. Yin, B. Xu, P. Li, N. An, Impact of pre-oxidation using H_2O_2 and ultraviolet/H_2O_2 on disinfection byproducts generated from chlor(am)ination of chloramphenicol, Chem. Eng. J. 317 (2017) 112–118.

[22] W.H. Chu, S.W. Krasner, N.Y. Gao, M.R. Templeton, D.Q. Yin, Contribution of the antibiotic chloramphenicol and its analogues as precursors of dichloroacetamide and other disinfection byproducts in drinking water, Environ. Sci. Technol. 50 (2015) 388–396.

[23] S.Q. Zhang, L.L. Wang, C.B. Liu, J.M. Luo, J.C. Crittenden, X. Liu, T. Cai, J.L. Yuan, Y. Pei, Y.T. Liu, Photocatalytic wastewater purification with simultaneous hydrogen production using MoS_2 QD-decorated hierarchical assembly of $ZnIn_2S_4$ on reduced graphene oxide photocatalyst, Water Res. 121 (2017) 11–19.

[24] C.W. Luo, J. Ma, J. Jiang, Y.Z. Liu, Y. Song, Y. Yang, Y.H. Guan, D.J. Wu, Simulation and comparative study on the oxidation kinetics of atrazine by UV/H_2O_2, UV/$HSO_5^-$and UV/$S_2O_8^{2-}$, Water Res. 80 (2015) 99–108.

[25] Y.J. Xiao, R.L. Fan, L.F. Zhang, R.D. Webster, T.-T. Lim, Photodegradation of iodinated trihalomethanes in aqueous solution by UV 254 irradiation, Water Res. 49 (2014) 275–285.

[26] N.V. Klassen, D. Marchington, H.C. McGowan, H_2O_2 determination by the I_3^- method and by $KMnO_4$ titration, Anal. Chem. 66 (1994) 2921–2925.

[27] W.H. Chu, N.Y. Gao, Y. Deng, S.W. Krasner, Precursors of dichloroacetamide, an emerging nitrogenous DBP formed during chlorination or chloramination, Environ. Sci. Technol. 44 (2010) 3908–3912.

[28] D. Liew, K.L. Linge, C.A. Joll, A. Heitz, J.W. Charrois, Determination of halonitromethanes and haloacetamides: An evaluation of sample preservation and analyte stability in drinking water, J. Chromatogr. A 1241 (2012) 117–122.

[29] J.Y. Fang, L. Ling, C. Shang, Kinetics and mechanisms of pH-dependent degradation of halonitromethanes by UV photolysis, Water Res. 47 (2013) 1257–1266.

[30] R.P. Schwarzenbach, P.M. Gschwend, D.M., Environ. Organic Chem. 34 (2003) 459–774.

[31] A. Zuorro, M. Fidaleo, M. Fidaleo, R. Lavecchia, Degradation and antibiotic activity reduction of chloramphenicol in aqueous solution by UV/H_2O_2 process, J. Environ. Manage. 133 (2014) 302–308.

[32] G. Mabilleau, S. Bourdon, M. Joly-Guillou, R. Filmon, M. Baslé, D. Chappard, Influence of fluoride, hydrogen peroxide and lactic acid on the corrosion resistance of commercially pure titanium, Acta Biomate 2 (2006) 121–129.

[33] B.E. Watt, A.T. Proudfoot, J.A. Vale, Hydrogen peroxide poisoning, Toxicol. Rev. 23 (2004) 51–57.

[34] W.H. Xu, G. Zhang, S.C. Zou, X.D. Li, Y.C. Liu, Determination of selected antibiotics in the Victoria Harbour and the Pearl River, South China using high-performance liquid chromatography-electrospray ionization tandem mass spectrometry, Environ. Pollut. 145 (2007) 672–679.

[35] USEPA, UV, Disinfection Guidance Manual - Draft, Office of Water, EPA 815-D-03-007, U.S Environmental Protection Agency: Washington DC, 2003.

[36] M. Kwon, S. Kim, Y. Yoon, Y. Jung, T.-M. Hwang, J. Lee, J.-W. Kang, Comparative evaluation of ibuprofen removal by UV/H_2O_2 and UV/$S_2O_8^{2-}$ processes for wastewater treatment, Chem. Eng. J. 269 (2015) 379–390.

[37] P. Westerhoff, S.P. Mezyk, W.J. Cooper, D. Minakata, Electron pulse radiolysis determination of hydroxyl radical rate constants with Suwannee River fulvic acid and other dissolved organic matter isolates, Environ. Sci. Technol. 41 (2007) 4640–4646.

[38] J. Porras, C. Bedoya, J. Silva-Agredo, A. Santamaría, J.J. Fernández, R.A. Torres-Palma, Role of humic substances in the degradation pathways and residual antibacterial activity during the photodecomposition of the antibiotic ciprofloxacin in water, Water Res. 94 (2016) 1–9.

[39] C.o. Neal, Alkalinity measurements within natural waters: towards a standardised approach, Sci. Total Environ. 265 (2001) 99–113.

[40] G.V. Buxton, C.L. Greenstock, W.P. Helman, A.B. Ross, Critical review of rate constants for reactions of hydrated electrons, hydrogen atoms and hydroxyl radicals (·OH/·O^-) in aqueous solution, J. Phys. Chem. Ref. Data 17 (1988) 513–886.

[41] Z.H. Zuo, Z.L. Cai, Y. Katsumura, N. Chitose, Y. Muroya, Reinvestigation of the acid–base equilibrium of the (bi)carbonate radical and pH dependence of its reactivity with inorganic reactants, Radiat. Phys. Chem. 55 (1999) 15–23.

[42] P.Z. Sun, W.N. Lee, R.C. Zhang, C.-H. Huang, Degradation of DEET and Caffeine under UV/Chlorine and Simulated Sunlight/Chlorine Conditions, Environ. Sci. Technol. 50 (2016) 13265–13273.

[43] Y. Yang, J.J. Pignatello, J. Ma, W.A. Mitch, Comparison of halide impacts on the efficiency of contaminant degradation by sulfate and hydroxyl radical-based advanced oxidation processes (AOPs), Environ. Sci. Technol. 48 (2014) 2344–2351.

[44] R.C. Zhang, P.Z. Sun, T.H. Boyer, L. Zhao, C.-H. Huang, Degradation of pharmaceuticals and metabolite in synthetic human urine by UV, UV/H_2O_2, and UV/PDS, Environ. Sci. Technol. 49 (2015) 3056–3066.

[45] T. Oppenländer, Photochemical purification of water and air: advanced oxidation processes (AOPs)-principles, reaction mechanisms, reactor concepts, John Wiley & Sons, 2003.

[46] O.S. Keen, N.G. Love, K.G. Linden, The role of effluent nitrate in trace organic chemical oxidation during UV disinfection, Water Res. 46 (2012) 5224–5234.

[47] P.Z. Sun, S.G. Pavlostathis, C.-H. Huang, Photodegradation of veterinary ionophore antibiotics under UV and solar irradiation, Environ. Sci. Technol. 48 (2014) 13188–13196.

[48] J. Mack, J.R. Bolton, Photochemistry of nitrite and nitrate in aqueous solution: a review, J. Photochem. Photobiol. A 128 (1999) 1–13.

[49] C.M. Sharpless, K.G. Linden, UV photolysis of nitrate: effects of natural organic matter and dissolved inorganic carbon and implications for UV water disinfection, Environ. Sci. Technol. 35 (2001) 2949–2955.

[50] R.C. Zhang, Y.K. Yang, C.-H. Huang, L. Zhao, P.Z. Sun, Kinetics and modeling of sulfonamide antibiotic degradation in wastewater and human urine by UV/H_2O_2 and UV/PDS, Water Res. 103 (2016) 283–292.

[51] Y.J. Xiao, L.F. Zhang, J.Q. Yue, R.D. Webster, T.-T. Lim, Kinetic modeling and energy efficiency of UV/H_2O_2 treatment of iodinated trihalomethanes, Water Res. 75 (2015) 259–269.

[52] P. Neta, R.W. Fessenden, Hydroxyl radical reactions with phenols and anilines as studied by electron spin resonance, J. Phys. Chem. 78 (1974) 523–529.

[53] C. von Sonntag, P. Dowideit, X.W. Fang, R. Mertens, X.M. Pan, M.N. Schuchmann, H.-P. Schuchmann, The fate of peroxyl radicals in aqueous solution, Water Sci. Technol. 35 (1997) 9–15.

[54] K. Li, P. Zhang, L. Ge, H. Ren, C. Yu, X. Chen, Y. Zhao, Concentration-dependent photodegradation kinetics and hydroxyl-radical oxidation of phenicol antibiotics, Chemosphere 111 (2014) 278–282.

[55] L. Hu, A.M. Stemig, K.H. Wammer, T.J. Strathmann, Oxidation of antibiotics during water treatment with potassium permanganate: reaction pathways and deactivation, Environ. Sci. Technol. 45 (2011) 3635–3642.

[56] K.S. Long, B.T. Porse, A conserved chloramphenicol binding site at the entrance to the ribosomal peptide exit tunnel, Nucleic Acids Res. 31 (2003) 7208–7215.

[57] B. Cédat, C. de Brauer, H. Métivier, N. Dumont, R. Tutundjan, Are UV photolysis and UV/H_2O_2 process efficient to treat estrogens in waters? Chemical and biological assessment at pilot scale, Water Res. 100 (2016) 357–366.

[58] X.H. Wang, A.Y.C. Lin, Phototransformation of cephalosporin antibiotics in an

aqueous environment results in higher toxicity, Environ. Sci. Technol. 46 (2012) 12417–12426.
[59] C.E. Jeffers, S.C. Tu, Differential transfers of reduced flavin cofactor and product by bacterial flavin reductase to luciferase, Biochemistry 40 (2001) 1749–1754.
[60] Z.T. Campbell, T.O. Baldwin, Fre is the major flavin reductase supporting bioluminescence from Vibrio harveyi luciferase in Escherichia coli, J. Biol. Chem. 284 (2009) 8322–8328.
[61] F. Chen, S.S. Liu, X.T. Duan, Molecular modeling study on the three-dimensional structure of the luciferase protein in Vibrio-qinghaiensis sp.-Q67, Acta Chim. Sinica 71 (2013) 1035–1040.
[62] M. Deborde, U. Von Gunten, Reactions of chlorine with inorganic and organic compounds during water treatment-kinetics and mechanisms: a critical review, Water Res. 42 (2008) 13–51.
[63] W.H. Chu, T.F. Chu, T. Bond, E. Du, Y.Q. Guo, N.Y. Gao, Impact of persulfate and ultraviolet light activated persulfate pre-oxidation on the formation of trihalomethanes, haloacetonitriles and halonitromethanes from the chlor (am) ination of three antibiotic chloramphenicols, Water Res. 93 (2016) 48–55.
[64] H.Y. Dong, Z.M. Qiang, J. Hu, J.H. Qu, Degradation of chloramphenicol by UV/chlorine treatment: Kinetics, mechanism and enhanced formation of halonitromethanes, Water Res. 121 (2017) 178–185.
[65] W.H. Chu, T.F. Chu, E.D. Du, D. Yang, Y.Q. Guo, N.Y. Gao, Increased formation of halomethanes during chlorination of chloramphenicol in drinking water by UV irradiation, persulfate oxidation, and combined UV/persulfate pre-treatments, Ecotoxicol. Environ. Saf. 124 (2016) 147–154.